Available online at www.sciencedirect.com
ScienceDirect
Trans. Nonferrous Met. Soc. China 25(2015) 3595−3603
Transactions of Nonferrous Metals Society of China
www.tnmsc.cn

Simulation of mechanical behavior of AZ31 magnesium alloy during twin-dominated large plastic deformation

Zhi-qiang WANG, Adrien CHAPUIS, Qing LIU

College of Materials Science and Engineering, Chongqing University, Chongqing 400044, China

Received 13 November 2014; accepted 17 June 2015

Abstract: Experiments and visco-plastic self-consistent (VPSC) simulations were used to quantify the amount of twinning and the relationship to stress−strain behavior in a textured Mg−3Al−1Zn plate. Two different compression directions were utilized to favor $\{10\bar{1}2\}$ extension or $\{10\bar{1}1\}$ compression twinning. $\{10\bar{1}2\}$ twins nucleate at the beginning of plastic deformation and grow to consume the parent grains completely. During compression along the normal direction, $\{10\bar{1}1\}$ twinning and $\{10\bar{1}1\}-\{10\bar{1}2\}$ double twinning start at strain of 0.05, and the number of twins increases until rupture, above strain of 0.15. $\{10\bar{1}1\}$ and $\{10\bar{1}1\}-\{10\bar{1}2\}$ twinning also occur during compression along the transverse direction, start at strain of 0.06 and then multiply in grains totally reoriented by $\{10\bar{1}2\}$ twins. Using suitable parameters, the VPSC model can accurately predict the occurrence of extension, compression and double-twinning as well as the flow stresses and deformed textures. According to VPSC simulations, twinning and slip have the same latent hardening parameters.

Key words: AZ31 magnesium alloy; twinning; crystal plasticity; plastic deformation

1 Introduction

Low density, good damping properties, high specific stiffness and strength make wrought magnesium alloys attractive lightweight structural materials in transportation applications. AZ31 magnesium alloy is one of the most widely used alloys, but its anisotropic and heterogeneous mechanical behavior dramatically hinders its applications. A key issue in the development and fabrication of magnesium alloys is the limited dislocation activity. Twinning has a tremendous effect on the mechanical behavior of AZ31 magnesium alloy at low temperature. The activated deformation modes highly depend on the orientations of the grains, and so depend on the texture, the deformation path and the mechanical process [1].

$\{10\bar{1}2\}$ extension twins [2] are activated during tension along the *c*-axis or compression normal to the *c*-axis. In favorably oriented grains, extension twins accommodate the deformation until they account for 80%−100% (volume fraction) [3−7]. The texture change induced by twinning is accompanied by a high degree of strain hardening [3−8].

$\{10\bar{1}1\}$ contraction twinning [9] induces texture softening, decreases the effective work hardening rate [10] and the flow stress [11], and is generally associated with early failure in tension [7,9,12]. Among the six possible variants, the experimentally observed $\{10\bar{1}1\}$ twin variants depend more greatly on the local strain accommodation than on the Schmid factor [10,13,14]. Thus, crystal plasticity models such as the visco-plastic self-consistent model (VPSC) [15] cannot accurately predict the observed twinning variants. The VPSC model also often fails to predict the observed $\{10\bar{1}1\}-\{10\bar{1}2\}$ secondary twin variant [12,16], whereas crystal plasticity coupled with finite element models can accurately model the stress state within contraction twins and predict the observed secondary extension twin variants [5].

Although many other crystal plasticity models are available and have shown very good accuracy, the VPSC approach [15] and the predominant twinning reorientation (PTR) scheme [17] are used to model large deformation with high twinning activity.

The VPSC has shown its ability to predict the texture development and deformation behavior when

Foundation item: Project (2013CB632204) supported by the National Basic Research Program of China; Project (51350110332) supported by the National Natural Science Foundation of China
Corresponding author: Adrien CHAPUIS; Tel: +86-23-65111295; E-mail: achapuis@cqu.edu.cn
DOI: 10.1016/S1003-6326(15)64000-6

strain is mainly accommodated by slip only [18−20] and slip plus extension twinning [8,21−27].

Although the work hardening behavior is complex, HUTCHINSON et al [28] proposed to simplify the hardening parameters as much as possible. But a curve-fitting approach based on this assumption (not presented in this paper) could not successfully model the anisotropic behavior during loading along different directions.

Twinning is often reported to increase the threshold stress of the slip systems. $\{10\bar{1}2\}$ twinning generates a Hall−Petch effect because of the twin boundaries. It can also produce dislocation transmutation during twin growth that changes the structure of the dislocations previously in the matrix [4,8,23,26]. The latent hardening parameters describe the additional hardening that the slip/twin systems experience due to twinning. In the previous studies, the latent hardening associated with extension twinning varied from 1.4 [8] to 4 [22]. Compression twins have also been reported to induce additional hardening because they generate boundaries that restrict the slip length of the dislocations [5].

Compression twinning is seldom incorporated in the VPSC simulations, with two notable exceptions: the study of AGNEW et al [8] where $\{10\bar{1}1\}$ twinning has been incorporated in the texture simulations of a Mg−Y alloy, and the study of OSTAPOVETS et al [27] to simulate the texture resulting from equal channel angular extrusion (ECAE).

Several studies follow the development of extension twins [5,6,29], but no systematic study follows and models compression twinning activity with strain, and moreover, $\{10\bar{1}1\}$ twinning is seldom modeled during large plastic deformations. This study aims to investigate and model plastic deformation with extension and compression twinning.

2 Experimental

The experimental material was a commercial AZ31 magnesium alloy (Mg−3%Al−1%Zn) (mass fraction) hot rolled plate (31 mm in thickness). The samples were spark cut and further annealed at 400 °C for 2 h to assure a soft O temper state, with a fully recrystallized texture which has as few dislocations as possible.

The texture of this initial AZ31-O material was measured by electron backscatter diffraction (EBSD), as shown in Fig. 1. The initial material had a typical basal texture with no preferential distribution of the $\{10\bar{1}0\}$ pole. The sample preparation consisted of mechanical polishing with a series of SiC papers down to a 4000-grit finish, followed by electro-polishing at 20 V and about −30 °C for 90 s using an AC2 commercial electrolyte (Struers, Denmark) and cleaning with ethanol. EBSD analysis was carried out on an FEI Nova 400 field emission gun-scanning electron microscope (FEG-SEM) equipped with an HKL channel 5 system. Another deformed sample was also been examined by EBSD to identify the type of twins.

Interrupted compression tests were carried out along the transverse direction (TD) and the normal direction (ND) at different strains. The compression samples were 10 mm high with a section of 7 mm × 8 mm. Mechanical tests were carried out on an AG-X 50 kN drawing machine at initial strain rate of 0.001 s^{-1}.

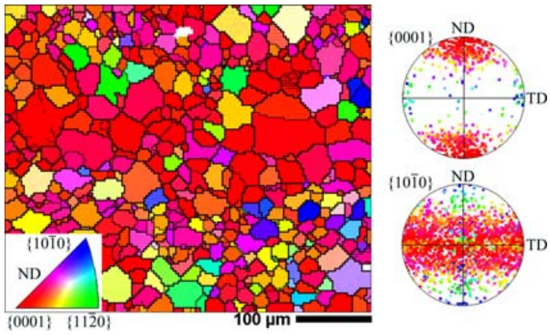

Fig. 1 Initial texture of AZ31 magnesium alloy rolled plate, and EBSD maps in ND−TD plane

To study twinning, investigations were performed on several samples compressed to different strains along TD and ND, referred as TD and ND samples in the following. These samples were examined by optical microscopy to reveal the twin activity. After mechanical grinding and electro-polishing, the surface was etched with an acetic-picral solution and observed with a ZEISS Axiovert 40MAT optical microscope. Initial and some deformed textures were measured by X-ray diffraction (XRD) on a D/max 2500 PC (Rigaku, Japan) with Cu K_α radiation.

In addition to the TD and ND samples, one sample was cut and compressed at an angle of 45° between TD and ND, and a tensile sample was tested to rupture along the TD. The tensile sample had a 10 mm gage length with a cross-section of 2 mm × 4 mm. The gage section of the tensile sample was manually polished to remove the surface defects that would promote crack initiation. An extensometer was used to measure the initial displacement in tension. In compression, the measured displacement was corrected to get the real strain.

TD, ND and 45° compression samples were also tested to rupture. These three compression samples along with the TD tensile sample were used to determine the material parameters by curve-fitting.

3 Experimental results

The experimental stress−strain curves during TD and ND uniaxial compression are recorded in Fig. 2. The

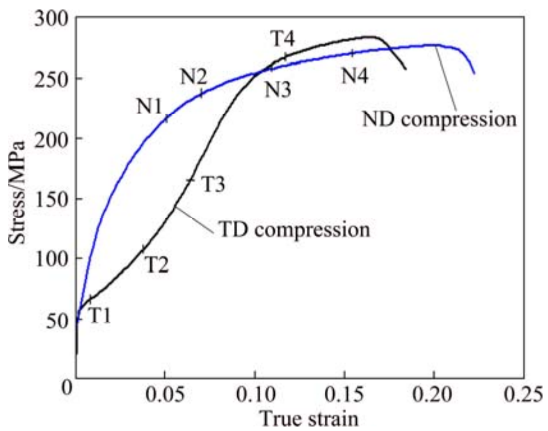

Fig. 2 Mechanical behaviors during ND and TD compression, and interrupted tests for observation

strains of different samples for which optical pictures were taken are shown on the curves. The compression along the TD direction was investigated at the following strains: ε(T1)=0.005, ε(T2)=0.042, ε(T3)=0.061 and ε(T4)=0.112. The corresponding microstructures are shown in Fig. 3. The compression along the ND direction was investigated at the fallowing strains: ε(N1)=0.04, ε(N2)=0.06, ε(N3)=0.095 and ε(N4)=14.5. The corresponding microstructures are shown in Fig. 4.

A sample was analyzed using EBSD to identify the type of twins (Fig. 5). Despite low deformation of the sample N2 (ε=0.06) and good index rate (80%), only a very few points are indexed within the thin bands, confirming the presence of $\{10\bar{1}1\}$ compression twins and $\{10\bar{1}1\}-\{10\bar{1}2\}$ double twins. On the other hand, the $\{10\bar{1}2\}$ extension twins are well indexed and wider. The band contrast map and the optical micrographs of samples after etching show very good similarities: the boundaries have a low contrast (or are not indexed) in the EBSD pattern, and are more heavily etched prior to optical observation, so, they appear dark in the two cases. Similar figures and analysis are available in Refs. [7,11].

During compression along the TD direction, $\{10\bar{1}2\}$ twinning is expected to be the main deformation mechanism. Many $\{10\bar{1}2\}$ twins with a typical lenticular shape are observable in Sample T1. These twins often have a different contrast compared with the matrix, and $\{10\bar{1}2\}$ twin boundaries are less etched than the grain boundaries, so, they appear thinner and less dark on the optical pictures. In Sample T1, 20%

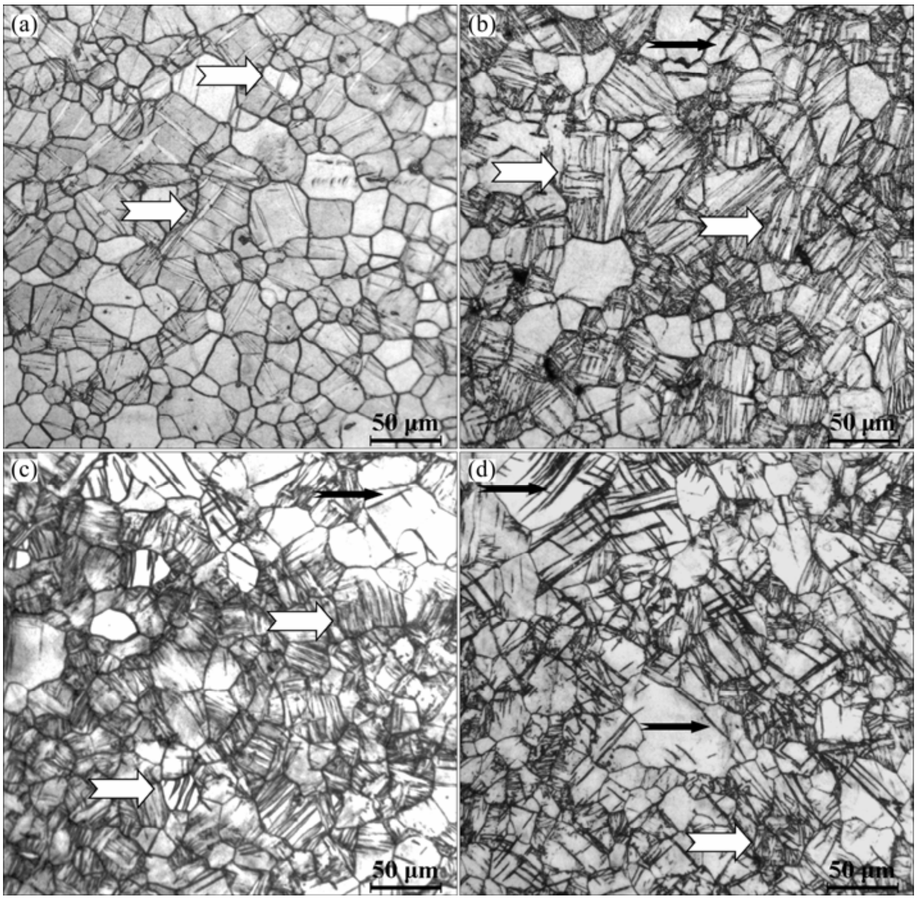

Fig. 3 Microstructures during TD compression at strain ε(T1)=0.005 (a), ε(T2)=0.042 (b), ε(T3)=0.061 (c) and ε(T4)=0.112 (d) (White arrows show some $\{10\bar{1}2\}$ extension twins, black arrows show some $\{10\bar{1}1\}$ compression twins and compression direction is horizontal)

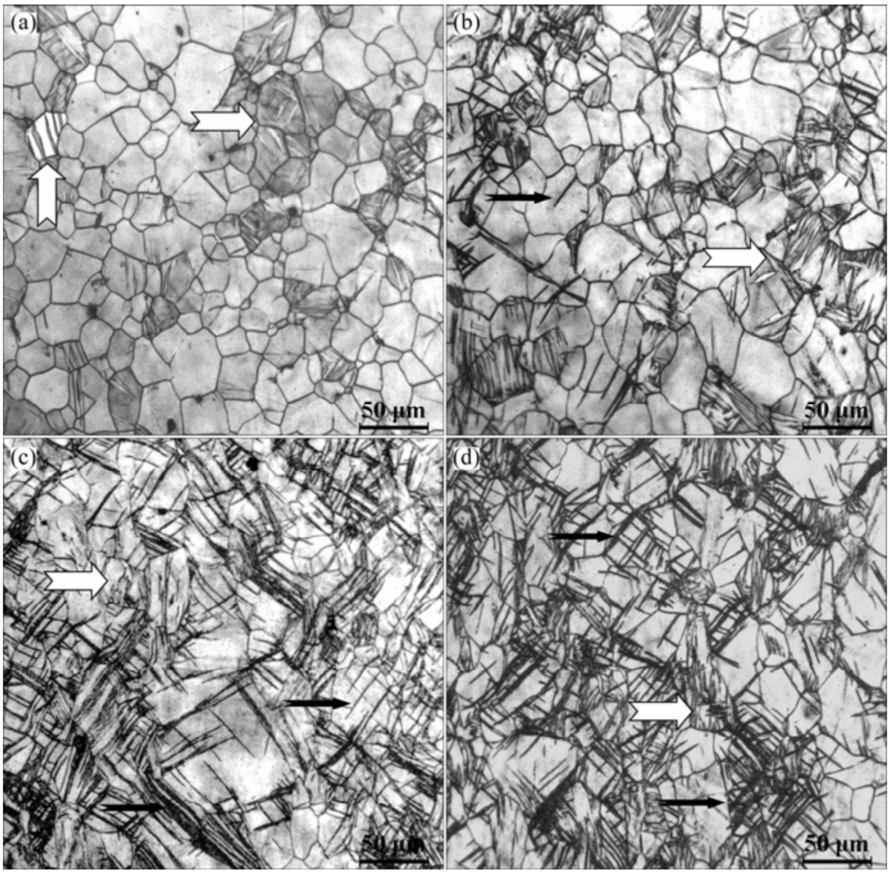

Fig. 4 Microstructures during ND compression at strain ε(N1)=0.04 (a), ε(N2)=0.06 (b), ε(N3)=0.095 (c) and ε(N4)=14.5 (d) (White arrows show some $\{10\bar{1}2\}$ extension twins, black arrows show some $\{10\bar{1}1\}$ compression twins and compression direction is horizontal)

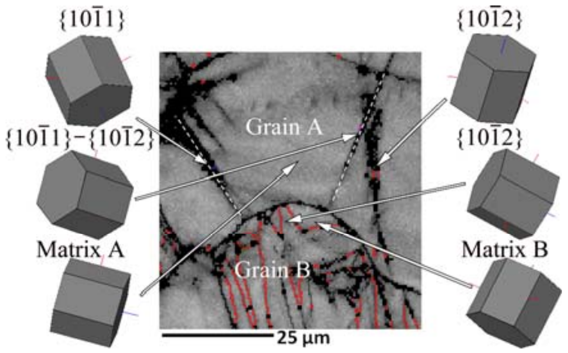

Fig. 5 Detail of EBSD-band contrast map performed on Sample N2, and schematic showing analysis of grains A and B containing twins (Compression twins are underlined with white dashed lines. Extension twin boundaries are colored in red. Compression direction is horizontal)

to 40% of grains have no twin, and about 20% of the grains are twin-free in Sample T2 after ε=0.04 compression. After ε=0.06 compression (Sample T3), when the stress reaches 160 MPa, a few compression twins are observed in grains where no extension twin boundaries are visible. Compression twins $\{10\bar{1}1\}$ and double twins are observable as straight dark lines on the optical pictures, and they are more heavily etched than the grain boundaries. It seems that these grains are deformed first by slip, then by compression twinning. In Sample T4, above 265 MPa, many compression twins are present in most of the grains. Some $\{10\bar{1}2\}$ twins are still visible in several grains; undoubtedly, $\{10\bar{1}1\}$ and $\{10\bar{1}1\}-\{10\bar{1}2\}$ twins occurring in grains are consumed by $\{10\bar{1}2\}$ twins, so, the material is consumed by secondary compression twins and tertiary twins [14].

During compression along ND, about 10% grains deformed by $\{10\bar{1}2\}$ twinning, as can be see from Fig. 4(a) after ε=0.04. These $\{10\bar{1}2\}$ twins certainly appear in grains with orientations far from the basal texture. A very few $\{10\bar{1}1\}$ thin compression twins are also visible. After ε=0.06, $\{10\bar{1}1\}$ twinning is clearly an active deformation mechanism. The number of twins increases with the increase of strain, and the multiplication of $\{10\bar{1}1\}$ twins is obvious whereas twin thickening seems to be negligible. Twin distribution throughout the sample is not homogeneous, and some areas in Sample N3 contain as many twins as that in Sample N4. Many grains contain several compression twin variants.

4 Modeling procedure

The simulations of stress–strain response and texture evolution were performed using the visco-plastic self-consistent (VPSC) model [15]. The inputs for the simulation were the experimentally measured initial texture which is discretized into 1000 grain orientations defined by three Euler angles, various parameters which govern the single crystal constitutive response (slip and twinning systems, critical resolved shear stress, and work hardening law) and the boundary conditions of the specified deformation. The model considers basal and prismatic slip of dislocations with ***a*** Burgers vectors, pyramidal slip of $\langle c+a\rangle$ dislocations, $\{10\bar{1}2\}$ extension twins and $\{10\bar{1}1\}$ contraction twins.

Some complete descriptions of the VPSC model are available in Refs. [15,25]. The relation between the average strain rate and stress, and the strain rate and stress in each grain can be linearized using different assumptions. The affine linearization is chosen, which has been shown to be the best in predicting the flow stress and the texture development [25].

The hardening responses of the individual slip and twinning systems are modeled by increasing the critical resolved shear stresses (CRSS), τ_0^{s}, for each deformation system "s", as a function of the total accumulated shear strain in the grain, Γ, according to an empirical Voce hardening rule:

$$\tau^{\mathrm{s}}=\tau_0^{\mathrm{s}}+(\tau_1^{\mathrm{s}}+\theta_1^{\mathrm{s}}\Gamma)\left[1-\exp\left(\frac{-\theta_0^{\mathrm{s}}\Gamma}{\tau_1^{\mathrm{s}}}\right)\right] \tag{1}$$

θ_0^{s} and θ_1^{s} are the initial and final slopes of the hardening curve, respectively. The initial shear strength (CRSS) is given by τ_0^{s}, while τ_1^{s} is back extrapolated from the asymptotic linear hardening region. All of these material parameters are summarized in Table 1.

To model twinning, the predominant twin reorientation (PTR) scheme proposed by TOMÉ et al [17] is used. The PTR prevents grain reorientation by twinning until a threshold volume fraction φ_{th1} is accumulated in any given system and rapidly raises the threshold to a value around $\varphi_{\mathrm{th1}}+\varphi_{\mathrm{th2}}$. In the PTR model, secondary twinning, such as $\{10\bar{1}1\}-\{10\bar{1}2\}$ double twinning, is allowed. The hardening due to twin boundaries or dislocations transmutation [26] can be indirectly included via higher latent hardening parameters associated with twin-slip interactions, as shown in Refs. [4,8,22]. In this study, all the self and latent hardening parameters are set to 1.

5 Modeling results

To model anisotropic deformation with the VPSC, the components of the velocity gradient L_{xx}, L_{yy}, L_{xz} and L_{yz} are not imposed during compression along z-axis, and the components L_{xx} and L_{yy} are not imposed during tension along z-axis. The CRSS and work hardening parameters for slip and twinning were fitted with four stress strain curves, as shown in Fig. 6. As the VPSC computes the stress for each plastic strain increment, the strain of the simulated curves is corrected to include plastic deformation. The present simulations use the optimized CRSS and hardening parameters summarized in Tables 1 and 2. Compared with other studies [24,25], the yield stresses as well as the initial CRSSs are lower. All latent hardening parameters are set to 1, without extra hardening due to twinning. The threshold stresses (CRSS) of twinning are also kept constant.

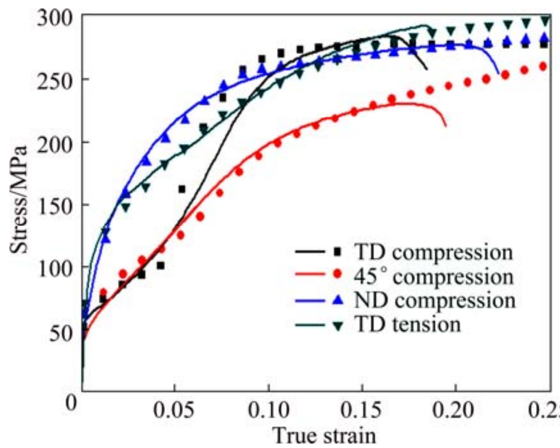

Fig. 6 Experimental (lines) and simulated (symbol) flow stress for four deformation paths

Table 1 AZ31-O temper material parameters for ship system used in VPSC simulations

Slip system	τ_0 (CRSS)/MPa	τ_1/MPa	θ_0/MPa	θ_1/MPa
Basal	1	9	200	90
Prismatic	50	40	3500	130
Pyramidal $\langle c+a\rangle$	60	160	3000	0

Table 2 AZ31-O temper material parameters for twinning system used in VPSC simulations

Twinning system	τ_0/MPa	φ_{th1}	φ_{th2}
$\{10\bar{1}2\}$	30	0.8	0.1
$\{10\bar{1}1\}$	205	0.01	0.09

The simulated slip and twinning system activities and the twin volume fractions are shown in Figs. 7 and 8, respectively. In both samples, basal slip is the main slip system. At ε=0.1, the simulated $\{10\bar{1}2\}$ twin volume fraction in the TD sample is 75%. In the ND sample, the $\{10\bar{1}2\}$ twin volume fraction is about 10% at ε=0.1, which is certainly due to the grains randomly oriented within the recrystallized initial texture. $\{10\bar{1}2\}$

extension twins have hard orientations compared with the matrix, so they do not deform until the whole matrix is consumed. Therefore, the threshold volume fraction $\varphi_{\rm th1}$ of $\{10\bar{1}2\}$ twinning is high and the simulated flow stress of TD compression dramatically increases in the strain range of 0.05−0.08 due to grain reorientation by twinning. Compression $\{10\bar{1}1\}$ twins are expected to appear at ε=0.06 during ND compression and at slightly higher strain during TD compression. The low threshold value $\varphi_{\rm th1}$ used to reorient grains into the $\{10\bar{1}1\}$ twin orientation allows the average stress to saturate and decrease rapidly, because compression twins have soft orientations compared with their matrix. Double twinning, i.e., $\{10\bar{1}1\}-\{10\bar{1}2\}$ twinning, is allowed in the model, so, at ε>0.10, the volume fraction of $\{10\bar{1}2\}$ twin increases again because of double twinning.

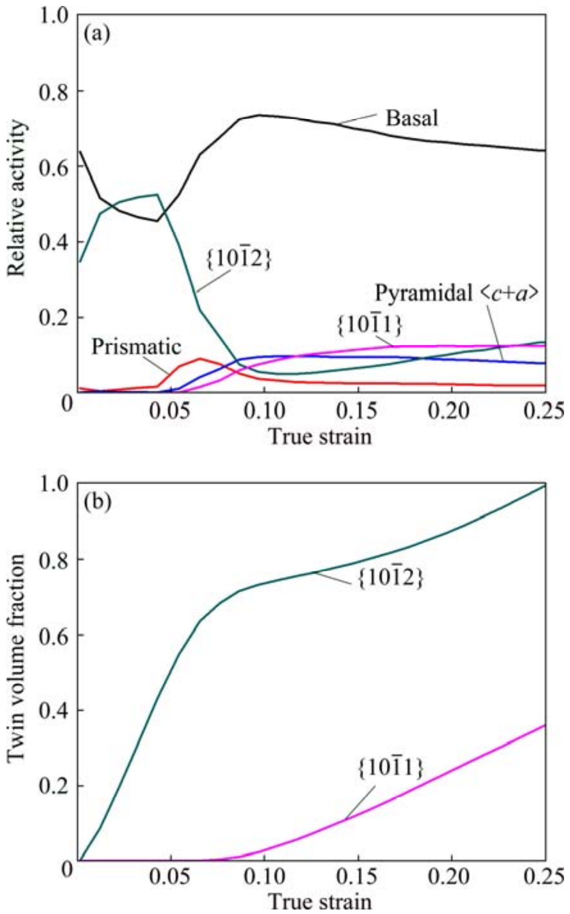

Fig. 7 Simulated relative slip and twin systems activity (a) and twin volume fraction (b) during TD compression

6 Discussion

The predicted amount of $\{10\bar{1}2\}$ twinning is in quantitative agreement with the observation, in which about 20% grains in the TD samples are twin-free at ε=0.04, whereas many grains seem to not be totally consumed by extension twins at ε=0.11. In both the TD and ND samples, $\{10\bar{1}1\}$ twins are present as thin lamellae within grains, easily seen after etching. These twins are observable and predicted at above strain of 0.06 in both samples, so, the CRSS and work hardening parameters modeling the AZ31 magnesium alloy behavior fit with the observation. $\{10\bar{1}1\}$ twins are much softer than the matrix, and the deformation concentrates in these twins, so that they do not thicken [16]. The occurrence of double twinning causes a loss of coherency of the twin−matrix boundary, which explains the non-lateral growth of the $\{10\bar{1}1\}$ twins. Compression twins and double twins are much softer, and more deformation happens within twins than within the matrix [9]. The deformation concentrates within these twins. They should provoke strong shearing at the grain boundaries and their extremities, leading to localized high non-compliant strain and failure [7,9,12]. But actually the total plastic strain accommodated by a material containing $\{10\bar{1}1\}$ twins is higher than 0.15. The sample compressed along TD was broken at strain of 0.16 and the sample compressed along ND was broken at strain of 0.20. The local strain accommodation at the junction of compression twins and grain boundary cannot be analyzed in the current study, but it seems that no cracks form despite the heterogeneous deformation.

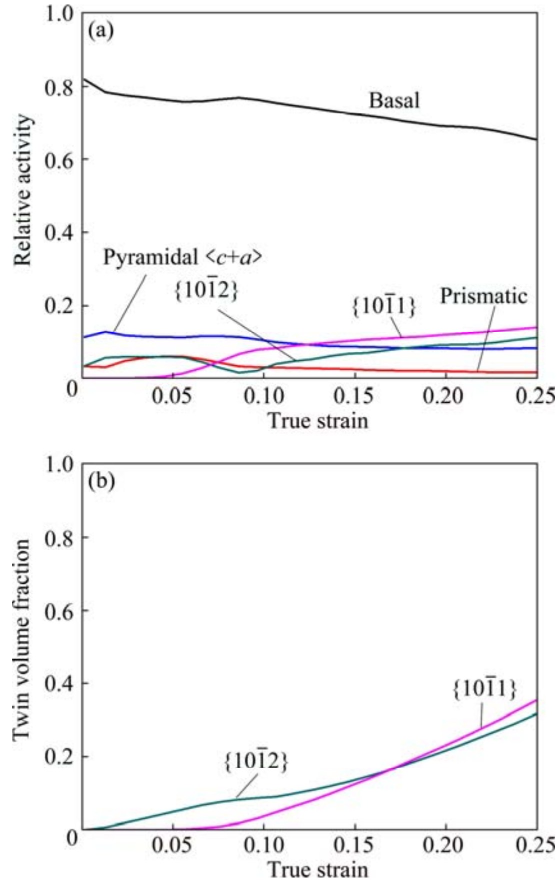

Fig. 8 Simulated relative slip and twin systems activity (a) and twin volume fraction (b) during ND compression

However, the macroscopic texture change can be predicted by the VPSC and measured by XRD. The simulations and measurements have been made at ε=0.11 in TD compression and ε=0.14 in ND compression, and the results are shown in Fig. 9. TD compression results in a full reorientation of the texture, as expected with $\{10\bar{1}2\}$ twinning. ND compression and $\{10\bar{1}1\}$ twins increase the intensity of the basal texture. The initial texture is a typical basal texture with c-axis close to ND but slightly tilted toward RD as in typical magnesium alloy cold rolled textures [30]. In the simulations, this distribution of c-axis slightly tilted toward RD persists even after TD and ND uniaxial compression, but this is not observable on the XRD figures.

Twins and double twins are seen as grains in modeling, and the PTR reorients the grains with the orientation of the dominant twin variant. As a result, the simulated texture, compared with the measured XRD texture, is stronger. Nevertheless, both simulations and XRD measurements confirm that the maximum intensity increases after TD and ND compression. Neither the model nor the experiments shows any preferential distribution of the prismatic plane.

7 Conclusions

1) $\{10\bar{1}2\}$ twinning occurs at the beginning of plastic deformation, and these twins consume and reorient the favorably oriented grains.

2) $\{10\bar{1}1\}$ twinning starts to be a deformation mechanism at stains of 0.05−0.06. The number of compression twins increases with increasing strain until rupture.

3) In compression, a total strain higher than 0.15 is accommodated when compression twinning is an important deformation mechanism. So, despite the strain localization within the compression twins, quite a lot of deformation can be accommodated before rupture.

4) Modeling with the VPSC can accurately predict the flow stress during large plastic deformation, as well as the twinning activity, the evolution of volume fractions of twins and the overall texture evolution.

5) In simulations, twinning does not generate extra hardening and slip does not need a higher latent hardening parameter from twin activity. In many other publications, slip needs a higher latent hardening parameter from extension twinning to fit the stress−strain curves.

6) At high strain, although the fractions of compression twins are similar, the experimental and simulated flow stress during ND compression is lower than that during TD compression.

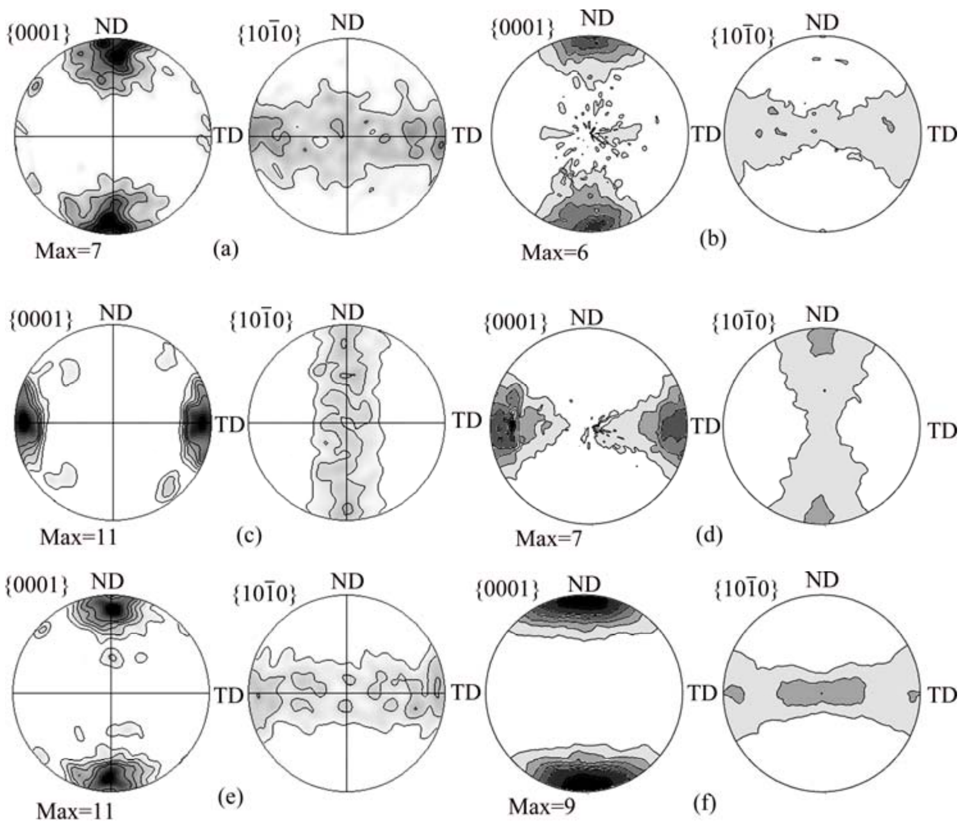

Fig. 9 Initial texture measured by EBSD (a) and XRD (b), textures after ε=0.11 TD compression simulated by VPSC (c) and measured by XRD (d) and textures after ε=0.14 ND compression simulated by VPSC (e) and measured by XRD (f) (Contour lines=1, 2, 3, 4, 5 ×random)

References

[1] WANG B S, XIN R L, HUANG G J, LIU Q. Effect of crystal orientation on the mechanical properties and strain hardening behavior of magnesium alloy AZ31 during uniaxial compression [J]. Materials Science and Engineering A, 2012, 534: 588−593.

[2] BARNETT M R. Twinning and the ductility of magnesium alloys. Part I: "Tension" twins [J]. Materials Science and Engineering A, 2007, 464(1−2): 1−7.

[3] BROWN D W, AGNEW S R, BOURKE M A M, HOLDEN T M, VOGEL S C, TOMÉ C N. Internal strain and texture evolution during deformation twinning in magnesium [J]. Materials Science and Engineering A, 2005, 399(1−2): 1−12.

[4] YI S B, DAVIES C H J, BROKMEIER H G, BOLMARO R E, KAINER K U, HOMEYER J. Deformation and texture evolution in AZ31 magnesium alloy during uniaxial loading [J]. Acta Materialia, 2006, 54(2): 549−562.

[5] KNEZEVIC M, LEVINSON A, HARRIS R, MISHRA R K, DOHERTY R D, KALIDINDI S R. Deformation twinning in AZ31: Influence on strain hardening and texture evolution [J]. Acta Materialia, 2010, 58(19): 6230−6242.

[6] HONG S G, PARK S H, LEE C S. Role of $\{10\bar{1}2\}$ twinning characteristics in the deformation behavior of a polycrystalline magnesium alloy [J]. Acta Materialia, 2010, 58(18): 5873−5885.

[7] CHUN Y B, DAVIES C H J. Twinning-induced negative strain rate sensitivity in wrought Mg alloy AZ31 [J]. Materials Science and Engineering A, 2011, 528(18): 5713−5722.

[8] AGNEW S R, YOO M H, TOMÉ C N. Application of texture simulation to understanding mechanical behavior of Mg and solid solution alloys containing Li or Y [J]. Acta Materialia, 2001, 49(20): 4277−4289.

[9] BARNETT M R. Twinning and the ductility of magnesium alloys. Part II: "Contraction" twins [J]. Materials Science and Engineering A, 2007, 464(1−2): 8−16.

[10] JONAS J J, MU S, AL-SAMMAN T, GOTTSTEIN G, JIANG L, MARTIN É. The role of strain accommodation during the variant selection of primary twins in magnesium [J]. Acta Materialia, 2011, 59(5): 2046−2056.

[11] JIANG L, SACHDEV A K, JONAS J J, MISHRA R K, GODET S, LUO A A. Twinning and texture development in two Mg alloys subjected to loading along three different strain paths [J]. Acta Materialia, 2007, 55(11): 3899−3910.

[12] CIZEC P, BARNETT M R. Characteristics of the contraction twins formed close to the fracture surface in Mg−3Al−1Zn alloy deformed in tension [J]. Scripta Materialia, 2008, 59(9): 959−962.

[13] LUO J R, GODFREY A, LIU W, LIU Q. Twinning behavior of a strongly basal textured AZ31 Mg alloy during warm rolling [J]. Acta Materialia, 2012, 60(5): 1986−1998.

[14] MU S, JONAS J J, GOTTSTEIN G. Variant selection of primary, secondary and tertiary twins in a deformed Mg alloy [J]. Acta Materialia, 2012, 60(5): 2043−2053.

[15] LEBENSOHN R A, TOMÉ C N. A self-consistent anisotropic approach for the simulation of plastic deformation and texture development of polycrystals: Application to zirconium alloys [J]. Acta Metallurgica et Materialia, 1993, 41(9): 2611−2624.

[16] BARNETT M R, KESHAVARZ Z, BEER A G, MA X. Non-schmid behaviour during secondary twinning in a polycrystalline magnesium alloy [J]. Acta Materialia, 2008, 56(1): 5−15.

[17] TOMÉ C N, LEBENSOHN R A, KOCKS U F. A model for texture development dominated by deformation twinning—Application to zirconium alloys [J]. Acta Metallurgica et Materialia, 1991, 39(11): 2667−2680.

[18] AGNEW S R, DUYGULU Ö. Plastic anisotropy and the role of non-basal slip in magnesium alloy AZ31B [J]. International Journal of Plasticity, 2005, 21(6): 1161−1193.

[19] BISWAS S, DHINWAL S S, SUWAS S. Room-temperature equal channel angular extrusion of pure magnesium [J]. Acta Materialia, 2010, 58(9): 3247−3261.

[20] ASKARI H, YOUNG J, FIELD D, KRIDLI G, LI D S, ZBIB H. A study of the hot and cold deformation of twin-roll cast magnesium alloy AZ31 [J]. Philosophical Magazine, 2014, 94(4): 381−403.

[21] BROWN D W, AGNEW S R, BOURKE M A M, HOLDEN T M, VOGEL S C, TOMÉ C N. Internal strain and texture evolution during deformation twinning in magnesium [J]. Materials Science and Engineering A, 2005, 399(1−2): 1−12.

[22] JAIN A, AGNEW S R. Modeling the temperature dependent effect of twinning on the behavior of magnesium alloy AZ31B sheet [J]. Materials Science and Engineering A, 2007, 25(1−2): 29−36.

[23] PROUST G, TOMÉ C N, JAIN A, AGNEW S R. Modeling the effect of twinning and detwinning during strain-path changes of magnesium alloy AZ31 [J]. International Journal of Plasticity, 2009, 25(5): 861−880.

[24] EBELING T, HARTIG Ch, LASER T, BORMANN R. Material law parameter determination of magnesium alloys [J]. Materials Science and Engineering A, 2009, 527(1−2): 272−280.

[25] WANG H, RAEISINIA B, WU P D, AGNEW S R, TOMÉ C N. Evaluation of self-consistent polycrystal plasticity models for magnesium alloy AZ31B sheet [J]. International Journal of Solids and Structures, 2010, 47(21): 2905−2917.

[26] OPPEDAL A L, EL KADIRI H, TOMÉ C N, VOGEL S C, HORSTEMEYER M F. Anisotropy in hexagonal close-packed structures: Improvements to crystal plasticity approaches applied to magnesium alloy [J]. Philosophical Magazine, 2013, 93(35): 4311−4330.

[27] OSTAPOVETS A, MOLNÁR P, JÄGER A. Visco-plastic self-consistent modelling of a grain boundary misorientation distribution after equal-channel angular pressing in an AZ31 magnesium alloy [J]. Journal of Materials Science, 2013, 48(27): 2123−2134.

[28] HUTCHINSON B, JAIN J, BARNETT M R. A minimum parameter approach to crystal plasticity modeling [J]. Acta Materialia, 2012, 60(15): 5391−5398.

[29] DOBRON P, CHMELIK F, YI S B, PARFENENKO K, LETZIG D, BOHLEN J. Grain size effects on deformation twinning in an extruded magnesium alloy tested in compression [J]. Scripta Materialia, 2011, 65(5): 424−427.

[30] STYCZYNSKI A, HARTIG Ch, BOHLEN J, LETZIG D. Cold rolling textures in AZ31 wrought magnesium alloy [J]. Scripta Materialia, 2004, 50(7): 943−947.

AZ31 镁合金在以孪生主导的塑性变形中力学行为的模拟

王志强，Adrien CHAPUIS，刘 庆

重庆大学 材料科学与工程学院，重庆 400044

摘 要：从实验和黏塑性自洽(VPSC)模拟两个方面定量分析具有织构的 AZ31 镁合金中孪晶数量及其与应力−应变曲线的关系。沿着两个不同的方向进行压缩以启动 $\{10\bar{1}2\}$ 拉伸或者 $\{10\bar{1}1\}$ 压缩孪生。$\{10\bar{1}2\}$ 拉伸孪晶在塑性变形的初始阶段形核并且长大到完全吞并母体。当沿着法向压缩时，$\{10\bar{1}1\}$ 孪生和 $\{10\bar{1}1\}-\{10\bar{1}2\}$ 二次孪生在应变量为 0.05 时开始启动，并且这些孪晶的数量一直增加直到材料断裂，即应变量大于 0.15。当沿着横向压缩应变量为 0.06 时，也会启动 $\{10\bar{1}1\}$ 孪生和 $\{10\bar{1}1\}-\{10\bar{1}2\}$ 二次孪生，然后在已经完全发生 $\{10\bar{1}2\}$ 孪生的晶粒中大量启动。应用适当的参数，VPSC 模型可以准确地判断拉伸孪晶、压缩孪晶和二次孪晶的启动和流动应力以及变形织构。从模拟中可以看出，孪生和滑移具有相同的硬化参数。

关键词：AZ31 镁合金；孪生；晶体塑性；塑性变形

(Edited by Mu-lan QIN)